JOURNAL OF PROPULSION AND POWER
Vol. 11, No. 1, January–February 1995

Numerical Experiments on the Vortex-Flame Interactions in a Jet Diffusion Flame

Fumiaki Takahashi*
University of Dayton, Dayton, Ohio 45469
and
Viswanath R. Katta†
Systems Research Laboratories, Inc., Dayton, Ohio 45440

Dynamic behavior of a laminar jet diffusion flame in response to an artificial vortex that issues radially from the fuel-jet core toward the flame zone has been studied numerically to illustrate essential physics of a naturally-forming shear layer vortex that has some radial velocity. A time-dependent, axisymmetric, implicit, third-order accurate numerical model is used with the infinitely-fast chemistry and unity Lewis number assumptions. A packet of fuel (methane) is ejected as a single-pulsed "side jet" at given initial and boundary conditions (the ejection velocity and period), which cover an order of magnitude in the time scale of the vortex-flame interaction. A vortex system with a pair of counter-rotating toroidal vortex rings is generated and penetrated into the high-temperature (highly viscous) layer with "solid-body" rotation. If the Peclet number *Pe* defined as the ratio of the characteristic diffusion to convection times, is small (the order of 10 or less), the vortex system pushes out the flame surface. If *Pe* is large (the order of 100), the vortex system nearly cuts through the high-temperature layer with a minimal flame movement, thus creating a significantly thin diffusive-thermal layer. In both cases, as the vortex approaches the flame surface, the net radial velocity of the incoming oxidizer stream crossing the flame and the reactants' diffusive fluxes into the flame increase. As a result, the flame structure similar to that of a strained counterflow diffusion flame is formed. A periodically-pulsed side jet has also been studied; the fuel packets ejected (at 500 Hz) induces the development of a large-scale vortex train in the shear layer of the primary jet, interacting with the flame zone.

Introduction

IN most combustion systems of practical interest such as gas turbine combustors and industrial furnaces, turbulence plays an important role in determining various aspects of performance and efficiency, because it provides the most effective means of stirring fluids and enhancing molecular mixing and reactions. However, flow visualization in combustion systems shows inhomogeneous stirring of fluids, composed of packets and parcels of fuel, oxidizer, and products, because of large-scale turbulent structures generated in the shear layer. Therefore, the interactions between the large vortices and the flame zone are of essential importance as they relate to various aspects of combustion phenomena such as the transition to turbulent flames, flame stability, and local extinction.[1-21]

In a jet diffusion flame for which the flame base is securely stabilized, the local flame extinction occurs near the laminar-to-turbulent flame transition point (breakpoint) as the fuel jet velocity is increased.[17] Takeno and Kotani[1] postulated for hydrogen flames that the local extinction is a result of the excess transport rate as compared to the reaction rate at the breakpoint. The event when the vortex was ejected radially and interfered with the flame zone was captured in methane flames by using flow visualization techniques.[5,8,9] Eickoff et al.[5] speculated that the diffusion flame was quenched because too much heat was diffused by the small-scale turbulence superimposed in these vortices. However, in the near-jet field of hydrocarbon-air flames, the flame zone is generally formed in the external fluid, not in the jet fluid, because of low stoichiometric fuel concentration and a high Damköhler number. It is, therefore, less likely that the flame zone interacts directly with the small-scale, high-intensity turbulence confined in the jet fluid.

A series of recent experiments[15,17,19-21] using a variety of diagnostic techniques revealed the essential features of the vortex-flame interactions that lead to the local extinction of methane jet diffusion flames. Figure 1 shows a schematic of

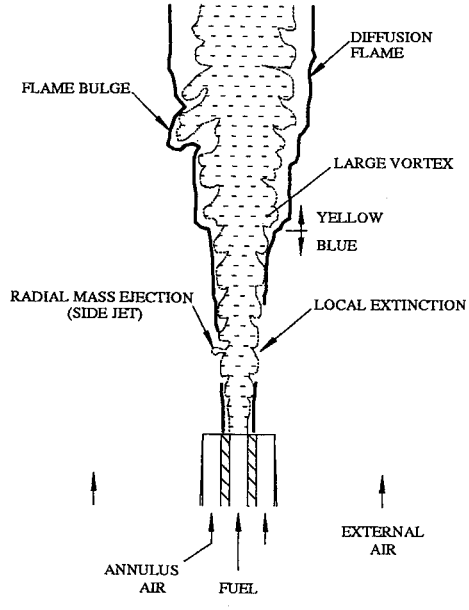

Fig. 1 Vortex-flame interactions observed in methane-air turbulent jet diffusion flames.

Presented as AIAA Paper 93-0456 at the AIAA 31st Aerospace Sciences Meeting and Exhibit, Reno, NV, Jan. 11–14, 1993; received Feb. 24, 1993; revision received March 21, 1994; accepted for publication April 14, 1994.

*Research Engineer, Research Institute, 300 College Park. Senior Member AIAA.

†Senior Engineer, Research Applications Division, 2800 Indian Ripple Road. Member AIAA.

some features of a locally extinguished turbulent flame based on the flow visualization.[17,19,20] In the near-exit region (less than several jet diameters), the flame zone is close to the jet-fluid core and is blue in color. The flame zone shifts away from the core downstream and becomes yellow because of the soot formation. The local extinction occurs in the blue flame region near the jet exit when fuel packets, conveyed by the large-scale vortices or more rapid radial mass ejection (side jet), reach the flame zone location. The flame bulge is observed generally downstream (typically more than 10 jet diameters) in the yellow flame region. The time required for the fuel packet to reach the flame zone location in turbulent flames (typically less than 1 ms) is, at least, an order of magnitude shorter than the characteristic diffusion time required to re-establish the reactant concentration field (typically >10 ms).[19,20] In an axially-pulsed laminar flame,[21] the interaction between the flame zone and a large-scale vortex with a radial transit velocity of ~2 m/s occurred over a longer time (~10 ms), and the local quenching was observed near the leading edge of the vortex.

Recent developments of numerical models to simulate various aspects of the transient behavior of diffusion flames[21-26] enable more challenging numerical experiments on the dynamic vortex-flame interactions with sufficient accuracy. The computer code[21,24-26] used in this paper employs a time-dependent, axisymmetric, implicit, third-order accurate, upwind numerical scheme with assumptions of infinitely fast, one-step chemical kinetics and unity Lewis number. In laminar diffusion flames, the second Damköhler number, defined as the ratio of the mass source from chemistry to diffusive transport[27] (or the characteristic diffusion to chemical reaction times), is generally large, and therefore, the diffusion process is the rate-determining factor. As a vortex approaches the flame zone and the diffusion layer becomes thin (reducing the Damköhler number), finite-rate chemistry must become important in the process, eventually leading to local extinction. Because of the axisymmetry and infinitely fast chemistry assumptions, the current model cannot simulate the three-dimensional nature of a vortex, nor can the flame extinction condition. However, it must provide global information on the physical nature (fluid-dynamic and transport aspect) of the vortex-flame interaction before local extinction. This study attempts to simulate numerically the transient response of a laminar jet diffusion flame to an artificial vortex that issues from a side jet. The primary objective of this study is to gain a better understanding of essential physical features of the interactions between the flame zone and a naturally-forming shear-layer vortex that has some radial velocity.

Numerical Experiment

Numerical Scheme

The laminar diffusion flame considered in this article is formed between a central methane jet and a concentric annulus airflow. Time-dependent governing equations, expressed in cylindrical coordinates, consist of mass continuity, axial and radial momentum conservation, and two scalar conservation equations.[24,25] Shvab-Zel'dovich formulation,[28] in conjunction with the flame-sheet assumption, is utilized. Body-force term caused by the gravitational field is included in the axial momentum equation. The system of governing equations is completed by using the equation of state. Transport properties are considered to vary with temperature and species concentrations. Enthalpy of each species is calculated from polynomial curve-fits, whereas the viscosity of the individual species is estimated from Chapman-Enskog collision theory.[29] The binary diffusion coefficient between any two species on the fuel side of the flame is assumed to be identically equal to that of the fuel and nitrogen. Similarly, on the oxidizer side of the flame, it is made identical to that of the oxygen and nitrogen. The Chapman-Enskog theory and the Lennard-Jones potentials[29] have been used to estimate these two binary diffusion coefficients.

The finite difference form of the governing equations is constructed on a staggered grid system based on an implicit QUICKEST numerical scheme. It is third-order accurate in both space and time and has a very low numerical diffusion error. At every time-step, the pressure field is accurately calculated by solving the system of algebraic pressure Poisson equations simultaneously. An orthogonal grid system (Fig. 2) with rapidly expanding cell sizes in both z and r directions is utilized. The computational domain of 150 × 60 mm in axial z and radial r directions, respectively, is represented by a mesh system of 241 × 71. The i.d. of the fuel tube (d = 9.6 mm) is almost the same as that used in the experiments.[15,17,19,20] Grid lines are clustered near the burner lip and side jet locations. The outer boundaries of the computational domain are shifted sufficiently far enough to minimize the propagation of disturbances into the region of interest.

The initial and boundary conditions for the axial U and radial V velocities, and the scalar variables for species β_1 and energy β_2[24,25] at different flow boundaries are shown in Fig. 3. The fully developed pipe flow and flat-velocity profiles are used at the exits of the fuel tube and the annulus air channel, respectively. Along the burner-lip walls, no-slip boundary conditions are enforced. An extrapolation procedure with weighted zero- and first-order terms is used to estimate the flow variables on the outflow boundary. During the calculations, radial side jets are introduced from different locations in the flowfield.

Test Conditions

The primary test cases reported in this article are listed in Table 1. Case 1 represents a laminar jet diffusion flame with low velocities of the primary jet U_j, annulus air U_a, and side jet V_s, and a long pulse width t_s. At the grid points within the side jet, the radial component of the local velocity and the scalar variables are replaced by V_s, β_{1S} (= β_{1F}), and β_{2S} (= β_{2F}), respectively, for a time-period of t_s. The primary jet has a

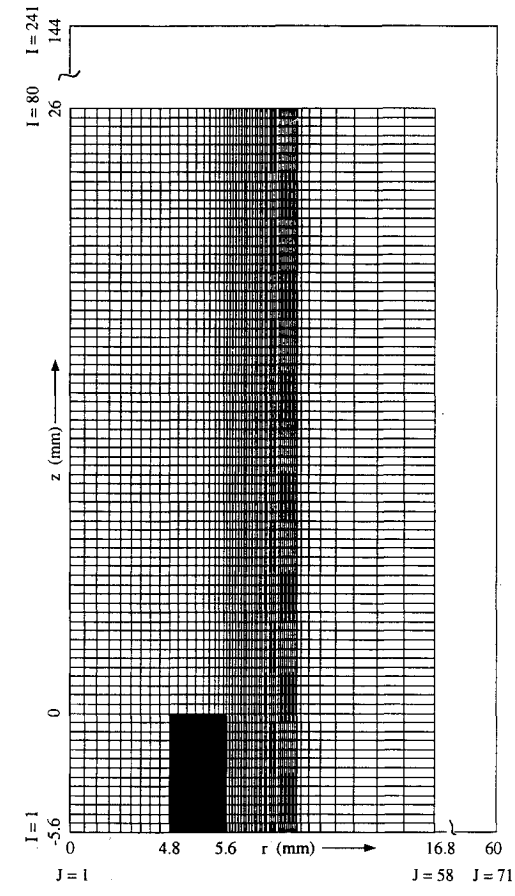

Fig. 2 Grid system.

Table 1 Test conditions

Case no.	Primary jet U_j, m/s	Primary jet Velocity profile	Annulus air U_a, m/s	Side jet r_s, mm	Side jet z_s, mm	Side jet V_s, m/s	Side jet t_s, μs	Side jet Pulse mode
1	1.5	Parabolic	1.5	4.8	14.2–16.5	2.0	300	Single-shot
2a	15	$\frac{1}{8}$th power	3	4.8	14.2–16.5	8.6	30	Single-shot
2b	15	$\frac{1}{8}$th power	3	4.8	14.2–16.5	8.6	60	Single-shot
2c	15	$\frac{1}{8}$th power	3	4.8	14.2–16.5	4.3	30	Single-shot
3	15	$\frac{1}{8}$th power	3	4.8	4.2–9.5	2.0	30	Periodic, 500 Hz

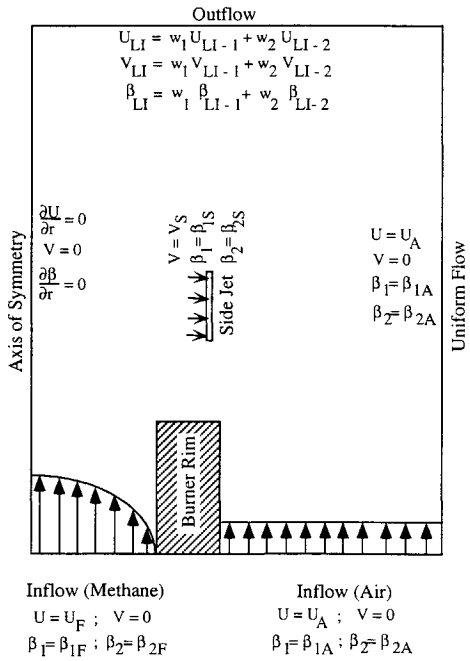

Fig. 3 Boundary conditions.

parabolic velocity distribution, representing the fully developed laminar pipe flow. The side-jet velocity in case 1 is the same magnitude as the radial velocity component of a large-scale vortex observed experimentally in the axially-pulsed laminar methane flame.[21] The radial location of the side jet ($r_s = d/2$) is nearly coincident with a dividing streamline between the jet and external fluids. The height of the side jet is chosen near the jet exit such that the flame zone interacts with the vortex intensely because of the flame proximity to the jet-fluid core. Case 2a represents a flame with higher velocities of the primary jet, annulus air, and side jet, and a shorter pulse width in consideration of a naturally-forming radial mass ejection observed in turbulent flames.[17,19,20] In the turbulent methane jet diffusion flame stabilized on a thick burner lip, the local flame extinction occurred at the mean primary jet velocity of ~15 m/s,[15,17] and the maximum radial velocity component (the mean plus three times the rms fluctuation) observed was ~7 m/s.[19] The velocity distribution of the primary jet is given by using the empirical equation of the $1/n$th-power law[30] for the fully developed turbulent pipe flow with the exponent $n = 6$ for a moderate Reynolds number (although the simulation considers laminar flows only). In case 2b, the pulse width of the side jet is doubled from case 2a to see the effect of the total mass ejected. In case 2c, the side jet velocity is halved from case 2a to test the effect of momentum at a same total mass ejection. Case 3 is an attempt to simulate a naturally-forming train of large-scale vortices in the shear layer, observed experimentally,[3,8,9,12,25] and their interaction with the flame zone. A moderate-speed periodically-pulsed (50% duty cycle) side jet is ejected into the flame under the condition of the same primary jet velocity as that in case 2a.

Results and Discussion

Single Vortex vs Flame Interactions

A steady-state solution for the diffusion flame structure without a side jet was obtained first for each case by numerous (typically several tens thousand times) iterative calculations using a long time step (~183 μs in case 1; ~37 μs in case 2). By using the steady-state solution as the initial condition, the temporal changes in the flame structure in response to the side-jet ejection were calculated using a short time step (~12.2 μs in case 1; ~2.4 μs in cases 2a–2c and 3). Figures 4 and 5 show the flame structure near the side jet for cases 1 and 2a, respectively: a color-coded mapping of the gas temperature T and a superimposed tracer particles image (Figs. 4a and 5a) and a color-coded mapping of the mole fractions of methane and oxygen X_{CH_4}, X_{O_2} with superimposed velocity vectors (Figs. 4b and 5b). The tracer particles in Figs. 4a and 5a were injected in front of the side jet (at $r = 4.9$ mm) over the axial distance of 4 mm at every time step. Notice that the elapse time after ejection t is an order of magnitude longer for case 1 ($t = 3.91$ ms) than case 2a $t = 0.391$ ms. Despite the difference in the magnitude of side-jet velocity and, in turn, the time scale of the process, the two cases show the following common features in the flame structures, because the vortex system formed dominates the global flow structure.

As a fuel packet issues from the side jet in the jet-fluid core toward the flame surface, a sudden change in the radial-velocity distribution near the edges of the side jet induces the roll-up of fluid and the subsequent formation of a vortex system composed of a pair of counter-rotating vortex rings. The vortex system grows as it engulfs surrounding gases and penetrates into a high-temperature (highly viscous) layer toward the flame surface. The vortex structure rotates as a whole naturally because of the uneven axial-velocity distribution in the shear layer. This tendency is more evident in case 2a because of its higher velocity gradient, and consequently, the upper portion of the double-vortex structure shrinks (Fig. 5a). The formation of the vortex structure with counter-rotating vortex rings and the subsequent solid-body rotation have been observed experimentally.[21] The vortex evolution processes described are depicted well by the injected particle images (such as Figs. 4a and 5a), and the consecutive time-series animation of the particle images and the color-coded temperature mappings on a computer display. The velocity vectors (Figs. 4b and 5b) show a zigzag motion (with respect to the stationary coordinate) typical of large-scale vortices. The rotating motion is more clearly seen in case 2a. The velocity vectors also show that the bulk flow comes into the upstream portion of the vortex system from the oxidizer side, crossing the flame surface, and goes out from the downstream portion, crossing the flame again. However, because the contribution of convection to the reactant fluxes vanishes at the flame surface (as will be described later), the reactant species enter the flame surface solely by diffusion from opposite directions, typical of diffusion flames.

Major differences in the response of the flame to the vortex movement between the two cases stem from the an-order-of-magnitude difference in the time scale of the process. In case 1, the vortex system pushes out the flame zone along with

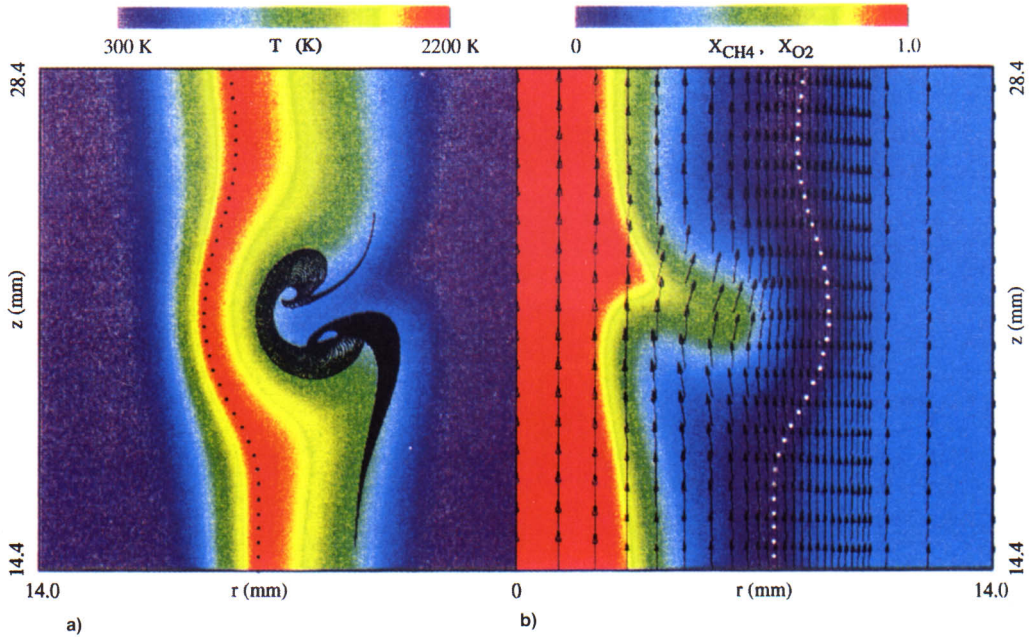

Fig. 4 Structure of a methane jet diffusion flame with a single side jet (case 1). t = 3.91 ms: a) temperature field and injected particles and b) mole fraction field of CH_4 and O_2 and velocity vectors.

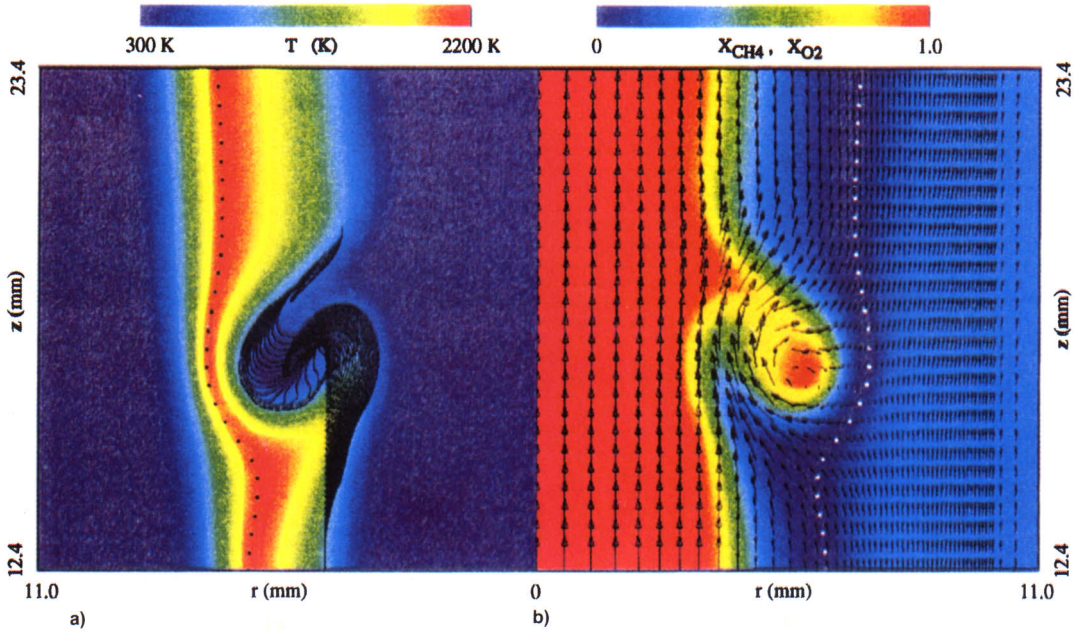

Fig. 5 Structure of a methane jet diffusion flame with a single side jet (case 2a). t = 0.391 ms: a) temperature field and injected particles and b) mole fraction field of CH_4 and O_2 and velocity vectors.

the isothermal layers well before the vortex leading edge reaches the initial flame surface location (Fig. 4a). By contrast, in case 2a, the vortex almost cuts across the high-temperature zone while the flame zone shifts slightly at a very last stage of the process (Fig. 5a). Consequently, the thermal layer ahead of the vortex becomes significantly thin as the leading edge of the vortex reaches the initial flame surface location. Furthermore, although the total mass ejected is more than twice of that in case 1, the methane mole fraction in the vortex system becomes lower than case 2a because of the excess diffusion of the fuel molecules to the surroundings over a longer elapse time (Figs. 4b and 5b).

Figures 6 and 7 show the radial distributions of the mean axial and radial velocity components (Figs. 6a and 7a); the gas temperature, the mole fractions of methane and oxygen (Figs. 6b and 7b); and the instantaneous total (axial and radial) mole fluxes of methane and oxygen by convection ($M_{CH_4,conv}$, $M_{O_2,conv}$) and diffusion ($M_{CH_4,diff}$, $M_{O_2,diff}$) at a height near the center of the vortex system for cases 1 and 2a, respectively (Figs. 6c and 7c). The results at t = 0 represent the steady-state solution. The radial location of the flame surface r_f at the height of the center of the side jet at t = 0 is ~7.3 mm in case 1, and ~6.5 mm in case 2a. For the lower velocity condition (case 1) at t = 0, the axial velocity component shows a velocity overshoot near the flame because of the buoyancy effect. That is not seen in case 2a, in which the external air velocity is ~3 m/s.

Because of the unity Lewis number assumption, heat transfer and mass diffusion processes must be similar. Therefore, the thickness of the layer in which the temperature varies is coincident with that for the (fuel and oxygen) mole fractions. The thickness of this layer (the diffusive-thermal layer) can be characterized using the full width at half-maximum (FWHM) of the temperature distribution w_T; w_T = 3.6 mm in case 1, and w_T = 2.4 mm in case 2a at t = 0. The higher primary jet and air velocity in case 2a result in a higher bulk flow velocity coming into the flame zone from the air side, pushing the contour of a stoichiometric mole-flux balance (where the flame surface is located) inward to the region where gradients of variables (velocity, temperature, and methane mole frac-

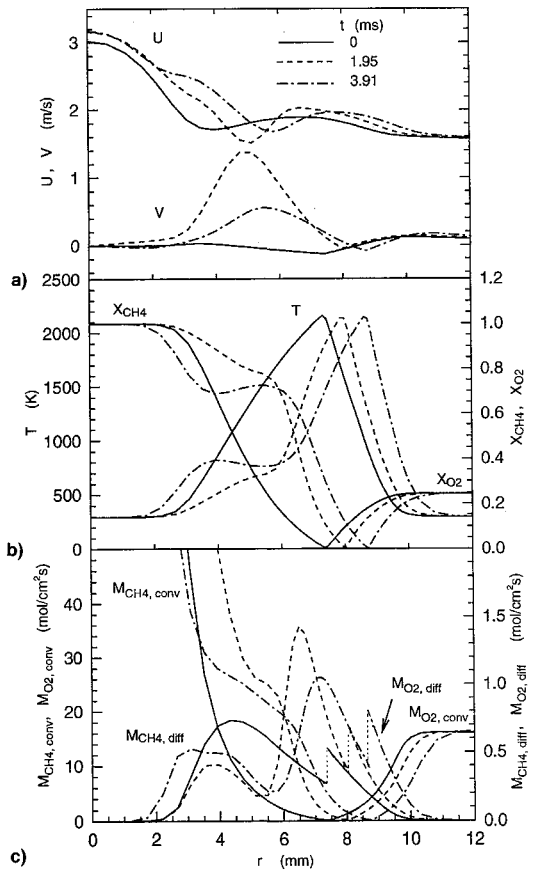

Fig. 6 Radial profiles of a) the axial and radial velocities; b) temperature, mole fractions of CH_4 and O_2; and c) mole fluxes of CH_4 and O_2 (case 1).

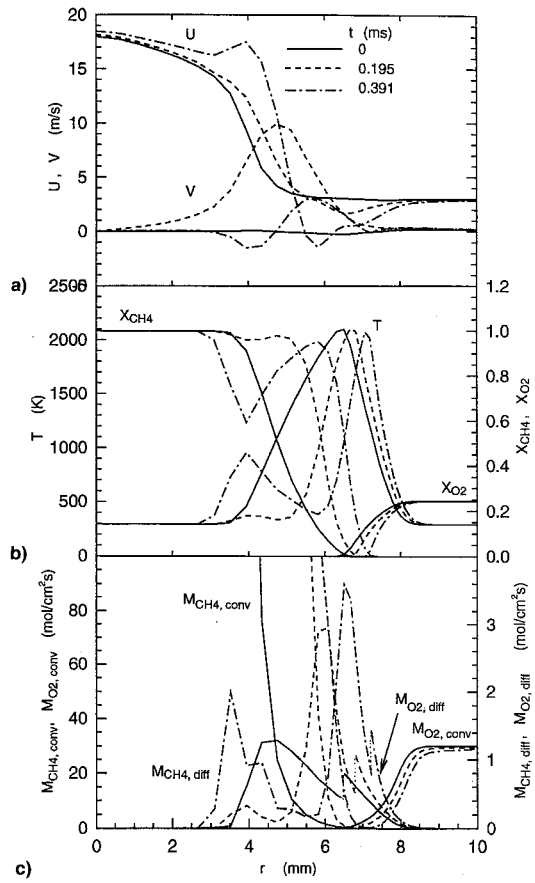

Fig. 7 Radial profiles of a) the axial and radial velocities; b) temperature, mole fractions of CH_4 and O_2; and c) mole fluxes of CH_4 and O_2 (case 2a).

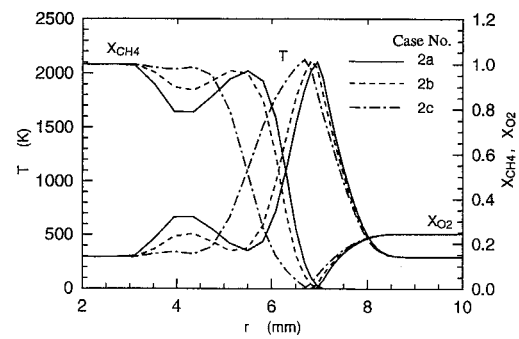

Fig. 8 Radial profiles of the temperature and mole fractions of CH_4 and O_2.

tion) are larger. Thus, the diffusive-thermal layer becomes thinner and the flame zone is more strained.

The magnitude of the instantaneous mole fluxes of the reactants by convection are large in the region away from the flame and decrease to zero at the flame surface, because the convection terms ($\rho_i Y_i v/W_i$, where ρ is density, Y is mass fraction, v is velocity vector, W is molecular weight, subscript i: species i for CH_4 and O_2) vanish as $Y_i \to 0$ at $r \to r_f$. On the other hand, the diffusion terms ($\rho_i D \nabla Y_i/W_i$) have finite values at $r = r_f$. The mole flux of methane by diffusion on the flame surface at $t = 0$ is $M_{CH_4,\text{diff}} = 0.27$ mole/m^{2}s ($M_{O_2,\text{diff}} = 0.54$ mole/m^{2}s) in case 1 and $M_{CH_4,\text{diff}} = 0.40$ mole/m^{2}s ($M_{O_2,\text{diff}} = 0.80$ mole/m^{2}s) in case 2a. Because of the null contribution of convection to the methane and oxygen mole fluxes at the flame surface, the diffusion contribution is always at a stoichiometric ratio (1:2). Incidentally, the oxygen mole flux determined experimentally[31] in the luminous zone near the base of a laminar diffusion flame of methane is ~1 mole/cm^{2}s.

At $t > 0$ in both cases, the peak temperature remains nearly constant (2100–2150 K), and a secondary temperature peak appears on the fuel side of the flame as a result of the roll-up of hot surrounding gases into the vortex structure. The diffusive-thermal layer becomes thinner ($w_T = 2.4$ mm at $t = 3.91$ ms in case 1, and $w_T = 1.0$ mm at $t = 0.391$ ms in case 2a), and the methane mole flux by diffusion increases with time ($M_{CH_4,\text{diff}} = 0.40$ mole/m^{2}s at $t = 3.91$ ms in case 1, and $M_{CH_4,\text{diff}} = 0.75$ mole/m^{2}s at $t = 0.391$ ms in case 2a). The reactant mole fluxes on the flame surface are thus almost proportional to w_T. In case 2a, in particular, the radial gradient of the methane mole fraction becomes significantly steep, thus resulting in the high methane flux diffusing into the flame zone (Fig. 7a).

Figure 8 shows the comparisons between the flame structures for cases 2a, 2b, and 2c at a fixed elapse time ($t = 0.293$ ms). In case 2b, the ejection period and, in turn, the total mass of the side jet is doubled from case 2a. Although the size of the vortex system becomes larger in the temperature field mapping (not shown) in case 2b, the structure remained similar because the vortex system penetrated into the hot zone at almost the same degree. In case 2c, the velocity of the side jet is halved under a fixed total mass. Because of the lower momentum of the vortex system in case 2c, it could not penetrate into the hot zone to reach the flame zone location and, thus, drifted away downstream.

If the movement of the vortex system toward the flame surface was extremely slow, changes in the fuel concentration by the movement would propagate around the vortex by diffusion simultaneously. As a result, a quasi-steady-state concentration field would be re-established in time, and thus, the flame surface would be shifted to a renewed equilibrated position. On the other hand, if the vortex speed was extremely fast compared to the rate required for the diffusion process, the surrounding concentration field would not be able to re-

spond to the changes except for a narrow region in the immediate vicinity of the vortex. Therefore, the Peclet number Pe for mass transfer, defined as the ratio of the convective to conductive (diffusive) mass transfer[27] (or the characteristic diffusion to convection times), must be an important dimensionless parameter in determining the degree of the vortex-flame interaction. Because of the unity Lewis number assumption, the Peclet number for mass transfer is identical to its counterpart for heat transfer.[27] In the previous paper,[19,20] the characteristic diffusion time τ_d, and the convection time caused by radial mass ejection τ_m were determined as $\tau_d = (\delta_d)^2/D$ (δ_d is diffusive transport layer thickness, D is diffusion coefficient), and $\tau_m = \delta_d/V_m$ (V_m is radial mass ejection velocity), respectively. Therefore, the Peclet number relevant to the side-jet ejection under current consideration becomes

$$Pe = (\tau_d/\tau_m) = (\delta_d V_m/D) \quad (1)$$

It was estimated[19,20] that $\tau_d \sim 30$ ms and $\tau_m \sim 0.2$ ms using $\delta_d \sim 1.5$ mm, $D \sim 0.7$ cm^2/s (methane at 1500 K), and $V_m = 6.6$ m/s, resulting in $Pe \sim 150$. By substituting $(r_f - r_s)$ at $t = 0$ for δ_d and V_s for V_m, for the flames under investigation in this article, $Pe \sim 71$ ($\tau_d \sim 89$ ms, $\tau_m \sim 1.25$ ms) was obtained for case 1, and $Pe \sim 209$ ($\tau_d \sim 41$ ms, $\tau_m \sim 0.2$ ms) for case 2a. Thus, the characteristic convection time is one to two orders of magnitude shorter than the characteristic diffusion (or heat transfer) time.

Figure 9 shows the temporal variations in the radial locations and transit velocities of the leading edge of the vortex system (r_l, V_l), the flame surface (r_f, V_f), and the width at half-maximum of the temperature distribution for cases 1 and 2a. As the vortex approaches the flame zone at $t < 2$ ms in case 1 (Fig. 9a), the vortex loses its speed while the flame surface gains its moving velocity. As the vortex pushes the flame, $(r_f - r_l)$ and w_T decrease and become nearly constant, and $V_l \approx V_f$ at $t > 2$ ms. Because of unity Lewis number, w_T is almost proportional to $(r_f - r_l)$. In case 2a (Fig. 9b), $(r_f - r_l)$, w_T, and V_l continue to decrease and V_f increases until the leading edge of the vortex reaches the initial flame zone location at $t \sim 0.4$ ms. The V_l curve changes its slope as the vortex starts the "solid-body" rotation described before.

Since the flame surface moves outward as the vortex system approaches, it is necessary to consider the net radial velocity

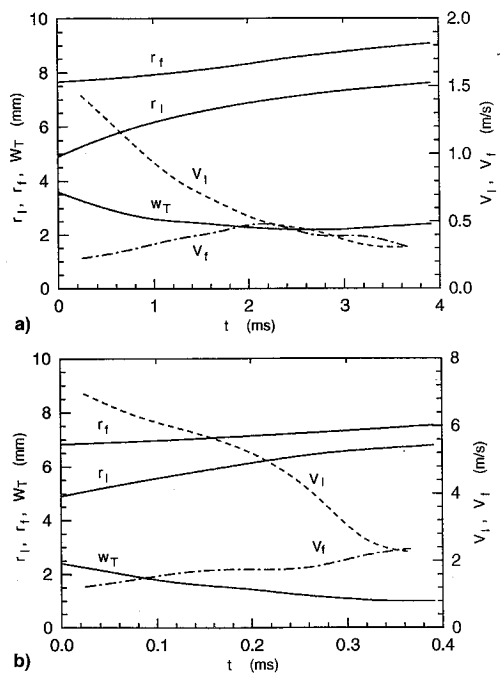

Fig. 9 Temporal variations in the radial locations and velocities of the vortex leading edge and flame surface and the FWHM of the temperature distribution: a) case 1 and b) case 2a.

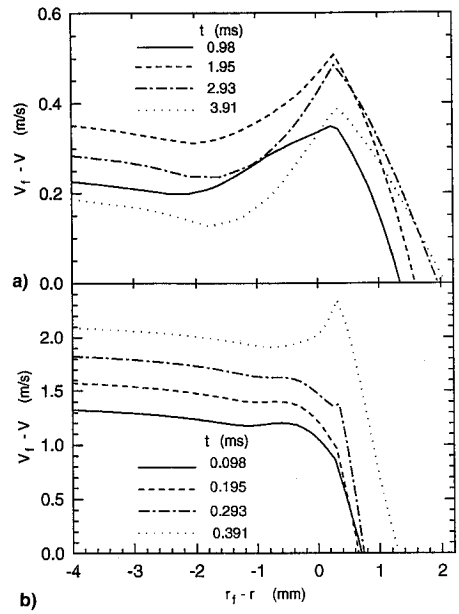

Fig. 10 Radial profiles of the net radial velocity relative to the flame surface.

component relative to the flame surface in order to examine the instantaneous structure near the flame. Figure 10 shows the relative radial velocity component $(V_f - V)$, which is positive for the incoming flow direction crossing the flame surface, as a function of the relative location $(r_f - r)$ in the near-flame region for cases 1 and 2a. In case 1 (Fig. 10a), as the vortex system approaches the flame surface, the profile of $(V_f - V)$ becomes similar to the one observed in strained counterflow diffusion flames[32,33] (with a peak at slightly downstream of the flame surface) at a relatively early stage of the vortex-flame interaction process. In case 2a (Fig. 10b), the temperature peak does not appear until a later stage of the process when the vortex leading edge approaches the close proximity of the flame surface and $(r_f - r_l)$ becomes constant. Because the velocity peak is caused by the longitudinal acceleration by gas expansion at high temperatures, the peak would not appear (or would be small, if any) if the gases (stream tubes) were able to expand laterally under a given flow configuration. Furthermore, unlike the counterflow diffusion flames, the velocity gradient (deceleration) of the approach flow just before entering the flame (which is normally used to assess the strain rate in the counterflow diffusion flames), is small because the net radial velocity component is nearly constant ($\sim V_f$) away from the flame surface as the actual velocity with respect to the laboratory coordinate is nearly zero. In jet diffusion flames, in general, the streamlines are nearly parallel to the flame surface (and thus, the velocity component perpendicular to the flame is small), while in counterflow diffusion flames, the streamlines are perpendicular for the stagnation-point flow. The radial side jet ejection has altered the normal jet diffusion flame structure. Therefore, the differences in the geometric configuration and velocity of the incoming flow play an important role in determining the flame structure, and a proper consideration needs to be made when applying a property (such as the critical strain rate for extinction) of one type of flames to another type.

Periodic-Vortices vs Flame Interactions

In case 3, the periodically-pulsed side jet induced the development of a train of large-scale vortices in the shear layer, similar to the structure observed experimentally.[8,9,12] A preliminary test showed that the evolution frequency of the large structure was ~500 Hz and nearly independent of the side jet frequency in the range of 500–1000 Hz. Figure 11 shows the structure of the flame with a periodic (500-Hz) side-jet ejection: a color-coded mapping of the temperature field (Fig.

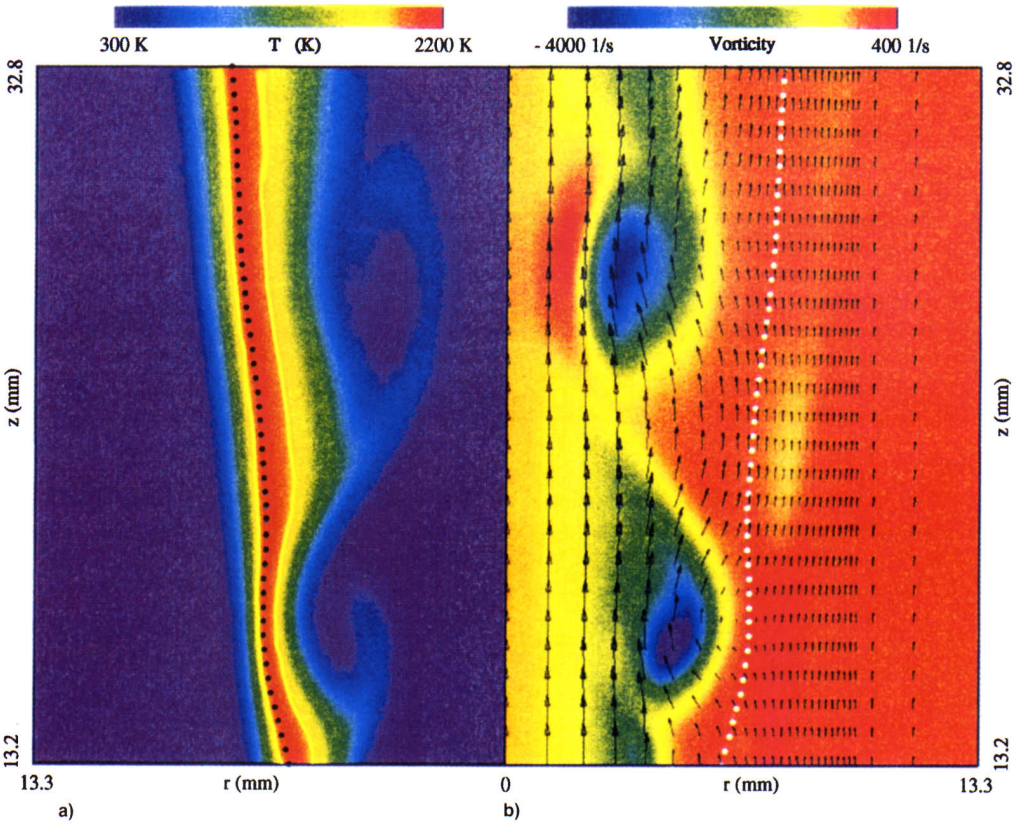

Fig. 11 Structure of a methane jet diffusion flame with a periodically-pulsed (500-Hz) side jet (case 3): a) temperature field and b) vorticity field and velocity vectors.

11a) and the vorticity field with superimposed velocity vectors (Fig. 11b). The temperature field image (Fig. 11a) shows the engulfment of the hot combustion products into the upstream side of the vortex and the thinned diffusive-thermal layer near the vortex upstream. Although the vortex interacts with the flame in a similar manner with the single-pulsed cases in the upstream region, the interaction becomes weaker downstream as the vortex loses its radial momentum and the distance between the vortex and the flame (or the diffusive-thermal layer thickness) increases. Unlike the single-shot side jet described before, the large vortex has the only one rotation direction as is normally seen in the shear layer. Thus, the vorticity (Fig. 11b) shows a negative peak. The velocity vectors again show a zigzag motion because of the large vortices.

Conclusions

A unique numerical experiment, in which a packet of fuel issues from a side jet toward a flame zone, has illustrated essential physics of the interactions between a large-scale vortex and a laminar diffusion flame. The following are among major conclusions.

The formation of a large-scale vortex structure composed of a pair of counter-rotating vortex rings and subsequent solid-body rotation of the vortex structure caused by the uneven axial-velocity distribution in the shear layer, observed experimentally, are simulated numerically. If the side-jet velocity (or momentum) is large, the vortex system penetrates into the high-temperature (highly viscous) layer; otherwise, it drifts away downstream before reaching the initial flame surface location. The level of penetration is nearly independent of the total mass ejected. The solid-body rotation of the vortex system is more evident in the higher primary jet velocity case because of the higher velocity gradient.

A Peclet number, defined as a ratio of the characteristic diffusion (or thermal conduction) to convection times for the side jet, is an important parameter in determining the level of the vortex-flame interactions. If *Pe* is small (the order of 10 or less), the vortex system pushes out the flame surface over the majority of the interaction period. If *Pe* is large (the order of 100), the vortex system nearly cuts through the high-temperature layer with a slight flame movement, thus resulting in an extremely thin diffusive-thermal layer with large gradients of the temperature and reactant concentrations. In both cases, as the vortex system approaches the flame surface, both the bulk flow velocity and the diffusive fluxes of reactants into the flame surface increase, and a flame structure becomes similar to that of a strained laminar counterflow diffusion flame. Therefore, the geometric flow configuration and incoming flow velocity, created by the large-scale vortex, are important factors in determining the flame structure.

The development of a train of large-scale vortices in the shear layer, observed experimentally, is simulated numerically by ejecting consecutive packets of fuel from the side jet periodically. Although the vortex-flame interactions similar to the single-pulsed cases take place in the upstream region, the level of the interactions decreases rapidly downstream, as the vortex loses its radial momentum.

Acknowledgments

This work was supported by the U.S. Air Force, Wright Laboratory, Aero Propulsion and Power Directorate, Fuels and Lubrication Division, Wright-Patterson Air Force Base, Ohio, under Contract F33615-92-C-2207 (Technical Monitor, C. W. Frayne). The authors would like to thank W. M. Roquemore for helpful discussions.

References

[1]Takeno, T., and Kotani, Y., "An Experimental Study on the Stability of Jet Diffusion Flames," *Acta Astronautica*, Vol. 2, 1975, pp. 999–1008.

[2]Yule, A. J., Chigier, N. A., Ralph, S., Boulderstone, R., and Ventura, J., "Combustion-Transition Interaction in a Jet Flame," *AIAA Journal*, Vol. 19, No. 6, 1981, pp. 752–760.

[3]Eickoff, H., "Instability and Coherent Structures in Jet Flames," *Recent Contributions to Fluid Mechanics*, edited by W. Haase, Sprin-

ger-Verlag, New York, 1982, pp. 50–57.

[4]Takahashi, F., Mizomoto, M., and Ikai, S., "Transition from Laminar to Turbulent Free Jet Diffusion Flames," *Combustion and Flame*, Vol. 48, No. 1, 1982, pp. 85–95.

[5]Eickoff, H., Lenze, B., and Leuckel, W., "Experimental Investigation on the Stabilization Mechanism of Jet Diffusion Flames," *Twentieth Symposium (International) on Combustion*, The Combustion Inst., Pittsburgh, PA, 1984, pp. 311–318.

[6]Gollahalli, S. R., Savas, Ö., Huang, R. F., and Rodriquez Azara, J. L., "Structure of Attached and Lifted Gas Jet Flames in Hysteresis Region," *Twenty-First Symposium (International) on Combustion*, The Combustion Inst., Pittsburgh, PA, 1988, pp. 1463–1471.

[7]Shekarchi, S., Savas, Ö., and Gollahalli, S. R., "Structure of a Split Gas Flame," *Combustion and Flame*, Vol. 73, 1988, pp. 221–232.

[8]Eickoff, H., Lehmann, B., Barsikow, B., and Winandy, A., "Instability of Ring Vortices and the Formation of Side Jets in Diffusion Flames and Hot Jets," 5th International Symposium on Flow Visualization, Prague, Czechoslovakia, Aug. 1989.

[9]Roquemore, W. M., Chen, L.-D., Goss, L. P., and Lynn, W. F., "The Structure of Jet Diffusion Flames," *Turbulent Reactive Flows*, edited by R. Borghi and S. N. B. Murthy, Springer-Verlag, Berlin, Vol. 40, 1989, pp. 49–63.

[10]Lewis, G. S., Cantwell, B. J., Vandsburger, U., and Bowman, C. T., "An Investigation of the Structure of a Laminar Non-Premixed Flame in an Unsteady Vortical Flow," *Twenty-Second Symposium (International) on Combustion*, The Combustion Inst., Pittsburgh, PA, 1989, p. 515.

[11]Gutmark, E., Parr, T. P., Parr, D. M., and Schadow, K. C., "Evolution of Vortical Structure in Flames," *Twenty-Second Symposium (International) on Combustion*, The Combustion Inst., Pittsburgh, PA, 1989, pp. 523–529.

[12]Chen, L.-D., Seaba, J. P., Roquemore, W. M., and Goss, L. P., "Buoyant Diffusion Flames," *Twenty-Second Symposium (International) on Combustion*, The Combustion Inst., Pittsburgh, PA, 1989, pp. 677–684.

[13]Coats, C. M., and Zhao, H., "Transition and Stability of Turbulent Jet Diffusion Flames," *Twenty-Second Symposium (International) on Combustion*, The Combustion Inst., Pittsburgh, PA, 1989, pp. 685–692.

[14]Takahashi, F., Mizomoto, M., Ikai, S., and Tsuruyama, K., "Stability Limits of Hydrogen/Air Coflow Jet Diffusion flames," AIAA Paper 90-0034, Jan. 1990.

[15]Takahashi, F., Schmoll, W. J., and Vangsness, M. D., "Effects of Swirl on the Stability and Turbulent Structure of Jet Diffusion Flames," AIAA Paper 90-0036, Jan. 1990.

[16]Pitts, W. M., "Large-Scale Turbulent Structures and the Stabilization of Lifted Turbulent Jet Diffusion Flames," *Twenty-Third Symposium (International) on Combustion*, The Combustion Inst., Pittsburgh, PA, 1991, pp. 661–668.

[17]Takahashi, F., and Schmoll, W. J., "Lifting Criteria of Jet Diffusion Flames," *Twenty-Third Symposium (International) on Combustion*, The Combustion Inst., Pittsburgh, PA, 1991, pp. 677–683.

[18]Chen, T. H., and Goss, L. P., "Statistical OH-Zone Structure of Turbulent Jet Flames from Liftoff to Near-Blowout," *Combustion Science Technology*, Vol. 79, 1991, pp. 311–324.

[19]Takahashi, F., and Goss, L. P., "Near-Field Turbulent Structures and the Local Extinction of Jet Diffusion Flames," *Twenty-Fourth Symposium (International) on Combustion*, The Combustion Inst., Pittsburgh, PA, 1992, pp. 351–359.

[20]Takahashi, F., and Vangsness, M. D., "Near-Field CARS Measurements and the Local Extinction of Turbulent Jet Diffusion Flames," *Dynamics of Heterogeneous Combustion and Reacting Systems*, edited by A. L. Kuhl, J.-C. Leyer, A. A. Borisov, and W. A. Sirignano, Vol. 152, Progress in Astronautics and Aeronautics, AIAA, Washington, DC, 1993, pp. 37–55.

[21]Hsu, K. Y., Chen, L. D., Katta, V. R., Goss, L. P., and Roquemore, W. M., "Experimental and Numerical Investigations of the Vortex-Flame Interactions in a Driven Jet Diffusion Flames," AIAA Paper 93-0455, Jan. 1993.

[22]Davis, R. W., Moore, E. F., Roquemore, W. M., Chen, L.-D., Vilimpoc, V., and Goss, L. P., "Preliminary Results of a Numerical-Experimental Study of the Dynamic Structure of a Buoyant Jet Diffusion Flames," *Combustion and Flame*, Vol. 83, Nos. 3/4, 1991, pp. 263–270.

[23]Ellzey, J. L., Laskey, K. J., and Oran, E. S., "Effects of Heat Release and Gravity on an Unsteady Diffusion Flame," *Twenty-Third Symposium (International) on Combustion*, The Combustion Inst., Pittsburgh, PA, 1991, pp. 1635–1640.

[24]Katta, V. R., Goss, L. P., and Roquemore, W. M., "Numerical Investigations of Transitional H2/N2 Jet Diffusion Flames," *AIAA Journal*, Vol. 32, No. 1, 1994, pp. 84–94.

[25]Katta, V. R., and Roquemore, W. M., "Role of Inner and Outer Structures in Transitional Jet Diffusion Flame," *Combustion and Flame*, Vol. 92, No. 2, 1993, pp. 274–282.

[26]Katta, V. R., Goss, L. P., and Roquemore, W. M., "Effect of Nonunity Lewis Number and Finite-Rate Chemistry on the Dynamics of a Hydrogen-Air Jet Diffusion Flames," *Combustion and Flame*, Vol. 96, Nos. 1/2, 1994, pp. 60–74.

[27]Strehlow, R. A., *Combustion Fundamentals*, McGraw-Hill, New York, 1984, p. 120.

[28]Williams, F. A., *Combustion Theory*, 2nd ed., The Benjamin/Cummings, Menlo Park, CA, 1985, p. 10.

[29]Hirschfelder, J. O., Curtis, C. F., and Bird, R. B., *The Molecular Theory of Gases and Liquids*, Wiley, New York, 1954.

[30]Schlichting, H., *Boundary-Layer Theory*, 7th ed., translated by J. Kestin, McGraw-Hill, New York, 1979, p. 599.

[31]Robson, K., and Wilson, M. J. G., "The Stability of Laminar Diffusion Flames of Methane," *Combustion and Flame*, Vol. 13, 1969, pp. 626–634.

[32]Tsuji, H., and Yamaoka, I., "Structure Analysis of Counterflow Diffusion Flames in the Forward Stagnation Region of a Porous Cylinder," *Thirteenth Symposium (International) on Combustion*, The Combustion Inst., Pittsburgh, PA, 1971, pp. 723–731.

[33]Chelliar, H. K., Law, C. K., Ueda, T., Smooke, M. D., and Williams, F. A., "An Experimental and Theoretical Investigation of the Dilution, Pressure and Flow-Field Effects on the Extinction Condition of Methane-Air-Nitrogen Diffusion Flames," *Twenty-Third Symposium (International) on Combustion*, The Combustion Inst., Pittsburgh, PA, 1991, pp. 503–511.